 doi:10.20944/preprints202002.0129.v1

Synthesis And Investigation of p-Ni-Doped rGO/n-TiO_2 Heterojunction Nanocomposite As An Efficient Catalyst for Photon-Induced Water Splitting

Ebraheim E. Ebraheim[1], Mohamed S. Atrees[2,*], , Mohammad S. Mahmoud[1,3], Hamed, M. Mira[2], M. Almutairi[1,4], Mohamed E. M. Ali[5] and Yasser M. khwassik [2]

[1] Chemical Engineering Department, Minia University, El-Menia, 61111, Egypt.

[2] Nuclear Materials Authority, Maadi Road, ElQattamia, Cairo, Egypt. P.O. 530.

[3] Collage of Applied Science, Department of Engineering, Suhar, 331, Oman

[4] Ministry of Electricity and Water, Kuwait, Kuwait, P.O.12010

[5] Water Pollution Research Department, Environmental Sciences Division, National Research Centre (NRC), Egypt, P.O. 12622

Corresponding author: *Mohamed S. Atrees ,

E-mail: smatreessemida@gmail.com ,Tel:+2027585832 and Fax+2027585831

Abstract

The present study focuses on the synthesis, characterization, and investigation of a p-n heterojunction photocatalysis. Titanium dioxide (TiO_2) can't alone induce the photocatalytic water splitting due to its wide bandgap, which decreases its catalytic activity in the visible light. To make redshift of absorptivity for the TiO_2, Nickel (Ni)-doped Graphene (rGO) supported TiO_2 was synthesized. Several characterization techniques have been employed to validate the composition and the light absorption ability of the prepared photocatalysts including TEM, SEM, EDS, XRD, XPS, and UV-Vis spectroscopy. The characterization revealed successful doping of the Ni and TiO_2 on the rGO nanosheet. Moreover, the UV-Vis spectroscopy indicated a significant shift of light absorption toward the visible spectrum. The photon-induced evolution of H_2 was remarkably enhanced using the prepared Ni-rGO/TiO_2 nanocomposite. Furthermore, the optimum ratio of rGO: TiO_2: Ni in the hybrids was 10:1:4, while the higher Ni ratio would decrease the photocatalytic activity. The stability of the photocatalyst was also verified during 8

 doi:10.20944/preprints202002.0129.v1

cycles of photocatalytic reactions. The kinetic study revealed the nature of the integrated reaction and the controlling step governing the reaction sequence.

Keywords:
Graphene; nanocomposite; photocatalyst; water splitting; hydrogen.

1. Introduction

Hydrogen is progressively gaining much attention as an alternative to fossil fuel [1]. The specific energy of hydrogen (141.9 kJ/g) is higher than that of gasoline 46.5 kJ/g and coal (30.2 kJ/g) [2, 3]. Typically, hydrogen is consumed in the proton exchange membrane (PEM) fuel cell, where it is supplied to the anode to tiger the anodic reaction through the fuel cell. Several routes are currently available for hydrogen production. Of them, photon-induced water breakdown using the solar beams is extensively studied. It is an attractive technology for producing clean and renewable energy without byproducts or pollution [4]. Principally, the photocatalysis reaction occurs in three steps: Excitation step, diffusion through the boundary layer, and surface transfer of photo-induced charge carriers. Accordingly, an efficient photocatalyst must satisfy several critical aspects related to its chemical properties, crystalline structure, and surface characteristics. However, semiconductors usually demonstrate deficiencies in its operation. Like so, it is thought-provoking to find a component that can alone fulfill all of these requirements. Although numerous semiconductors for water splitting have been studied in the last few decades, yet, their activity in a wide spectrum region needs more investigation. It is also evident that a single-component photocatalyst like TiO_2, cannot obtain the desirable photons to electron efficiency. A semiconductor heterojunction is typically formed by the direct contact of two layers of dissimilar crystalline semiconductors. This structure can promote the charge transfer of photocatalysts through several mechanisms including (i) direct hole mobility from the valence band and (ii)

Preprints (www.preprints.org) | NOT PEER-REVIEWED | Posted: 10 February 2020 doi:10.20944/preprints202002.0129.v1

indirect hole transfer through the surface states [5]. When two dissimilar semiconductors are combined, the charge transfer by e/h pair can prolong the lifetime of the e/h charge carriers. As a result, permitting extra time for the photocatalytic process. Furthermore, the bandgap of the dissimilar semiconductor should be as close to the water cleavage range as possible so as to extend the energy range of photo-excitation for the system.

Theoretically, when photons with energy $hv>E_{gap}$ are absorbed by a semiconductor during the photoelectrochemical process, electrons are excited through the forbidden bandgap, producing the e/h pairs. For a heterojunction initially held at the equilibrium potential, the local concentrations of e/h will be shifted from the equilibrium values. This will cause a split of the Fermi level into several quasi-Fermi levels. Meanwhile, the holes generated by photoexcitation process can accept electrons from the adsorbed water molecule, electron flow proceeds and a photocurrent is generated. The intensity of that current depends on the generation, collection, and reaction of holes in the heterojunction interface. It is evident that the driving force for the e/h movement is the gradient of the correct quasi-Fermi level. The current density is therefore given by [6]:

$$j = j_n + j_p = nu_n\left(\frac{\partial E_{Fn}}{\partial x}\right) + pu_p\left(\frac{\partial E_{Fp}}{\partial x}\right) = nu_n\left(\frac{\partial \overline{\mu_n}}{\partial x}\right) + pu_p\left(\frac{\partial \overline{\mu_p}}{\partial x}\right) \quad (1)$$

where n and p are the concentrations and u_n and u_p are the mobilities of electrons and holes. Remembering that the electrochemical potential can be separated conceptually into chemical and electrical parts, often referred to as “drift-diffusion” models.

The of the electron/hole pair recombination time is calculated using equation [7]:

$$\tau_{rec} = \frac{\Delta n}{R} \quad (2)$$

Preprints (www.preprints.org) | NOT PEER-REVIEWED | Posted: 10 February 2020 doi:10.20944/preprints202002.0129.v1

where Δn is the excess carrier density (cm^{-3}) and R is the rate of recombination of the excess carriers given by:

$$R = \frac{-d\Delta n}{dt}, \text{ sec}^{-1} \quad (3)$$

Furthermore, Martina De Laurentis and Andrea Irace [6] signposted that the e/h rejoin can be handled only by the quantum mechanical calculations. As it includes shifts between active states, it is intrinsic that the rate of recombination of e/h solely relies on the likelihood of occupation of the energy levels. Thus, it depends on (i) the energy, (ii) the temperature, (iii) the e/h concentration, and (iv) the excess carriers Δn. Generally, the e/h recombination has a trivial impact on the bandgap energy, suggesting that by increasing the e/h lifetime, high photocatalytic activity is expected, which is also consistent with the previous reports [8, 9].

Titanium dioxide (TiO_2) is frequently studied as a stable photocatalyst for water splitting reactions [10, 11]. It embraces several merits as a photocatalyst, like remarkable optical and electronic properties, good stability, activity to both light and aqueous solutions, and its robust oxidizing ability [12]. Even so, TiO_2 possesses a relatively long band gap (3.2 eV), thus, it is preferably used to conduct the photochemical reaction in the ultraviolet (UV) light region [13]. In addition, it has been reported that the recombination of the e/h pairs is noticed upon the excitation of TiO_2 photo catalyst. These hurdles slowed down the practical applications as a photocatalyst. Accordingly, numerous works have been dedicated to reducing the bandgap of TiO_2 to grasp as much visible light spectrum as possible. Doping the TiO_2 with one of the transition metal oxides, (like Fe; Zn; Cu; Ni; and V), leads to a decrease in the photocatalyst bandgap [8, 9, 14, 15]. In addition, construction of a photocatalyst containing TiO_2, a non-metal (C,

 doi:10.20944/preprints202002.0129.v1

S, and N), and metal (Fe, Ni, and Cr) can form extra acceptor and donor states above and below the valence and conduction bands, respectively [16, 17].

Contrariwise, doping of carbon nanostructures like nanotubes (CNTs), reduced graphene oxide sheets (rGO), and functional graphene sheet (FGs) with TiO_2 have been investigated. It was found that doping of carbon nanostructure with TiO_2 not only improves the photocatalytic activity but also provides extra electron acceptors sites that enhance the overall photo-conversion efficiency [18, 19, 20, 21]. Due to its high work function (4.42 eV) [22], graphene can accept photogenerated electrons from the CBs of most semiconductors without barriers, which will efficiently conquer the recombination of e/h pair and significantly enhance their reaction ability. Furthermore, graphene has a relatevily high electrical conductivity. Therefore, the electron's mobility is very fast across the rGO sheet that causes electrons to reach the active sites for H_2 evolution. Accordingly, numerous researches emphathized on the role of rGO to enhance the H_2 production activity, and many promising results are achieved using rGO phohotocatalyst in both UV and visible light-active systems [4, 11, 18-20]. The TiO_2/rGO photocatalyst has been intensely investigated to detect the best TiO_2/rGO ratio for photocatalytic H_2 production. For instance, X. Y. Zhang et. al [23] investigated the photocatalytic activity of rGO/TiO_2 with a different weight ratio of rGO. They indicated that by increasing the content of rGO, the H_2 production rate increases to the highest value at rGO ratio of 10%. Further increase of rGO leads to a decrease in its photocatalytic activity due to the introduction of the e/h recombination centers into the composite [23]. Similar results were obtained in the hydrothermal prepared rGO/TiO_2 photocatalysts by the same group [24]. They concluded that the photocatalytic property was enhanced due to the role of rGO as an electron acceptor and transporter. On the other

Preprints (www.preprints.org) | NOT PEER-REVIEWED | Posted: 10 February 2020 doi:10.20944/preprints202002.0129.v1

terminal of the heterojunction photocatalyst, another dopant should be able to act as an electron donor during the hydrogen evolution reaction.

In this study, the synergistic doping of the p-Ni /n-TiO_2 nanoparticles over the substrate of rGO has been investigated to enhance the PC activity toward H_2 production from water. The study is aimed at selecting the suitable ratio of Ni dopant to TiO_2 and rGO. The catalytic activity of Ni /TiO_2 supported on rGO depends on the preparation methods of the catalysts. In addition, a kinetic study has been conducted to verify the dependence of the apparent reaction rate on the reaction temperature.

2. Experimental

2.1 Preparation of the photocatalyst

2.1.1 Preparation of GO

A simple process to prepare Graphene oxide (GO) in the laboratory is the modified Hummers method. First, two grams of graphite powder (Sigma Aldrich Co., powder, <20 µm, synthetic) and one gram of sodium nitrate are mixed with a 9:1 mixture of H_3PO_4:H_2SO_4. The process is done in an ice bath to control the reaction temperature. Second, adding 12 g of $KMnO_4$ to the mixture carefully while stirring. Then, the stirring continues for an hour at a temperature of 35 ^oC. Subsequently, H_2O_2 and distilled water were added to the mixture while stirring for 30 min to precipitate brownish-yellow GO.

2.1.2 Fabrication of Ni-doped rGO/TiO_2 nanocomposites

The following steps are implemented to prepare the photocatalyst. First, dispersing one gram of GO in 50 ml ethanol by stirring. Then, sonication is done for 30 minutes. Afterward, a suitable amount of the Ni acetate was added to the mixture solution and boiled under reflux at 150 ^oC for 10 h. Consequently, the solution was filtrated to collect the filtrate, which is mixed with a proper

Preprints (www.preprints.org) | NOT PEER-REVIEWED | Posted: 10 February 2020 doi:10.20944/preprints202002.0129.v1

mass of the precursor of TiO_2 (titanium tetra isopropoxide). After drying, samples were calcined at 800 ^oC for 3 hours. In these experiments, the mass of rGO and TiO_2 was fixed, and the mass of transition metal nanoparticles varies in such a way that the mass ratio is (rGO:TiO_2: Ni = 10: 1: (1 to 5)).

2.2 Characterization of physical properties

The surface characteristics and the degree of crystallinity of the prepared nanocomposite were determined using X-ray diffraction (Rigaku Co, Japan). It has an incident ray (λ = 1.54056 Å) and a scan rate of 0.05 s^{-1} over a 2θ range from 5 to 80^o. Moreover, a high-resolution image of the rGO sheets hosting Ni and TiO_2 has been captured using a 200 kV-beamed transmission electron microscopy (TEM, JEOL Ltd. Japan). The percentage of each atom appearing in the rGO:Ni: TiO_2 nanocomposite samples were obtained using X-ray Microanalysis (TEAM™ EDS analysis, EDAX Ltd.). The light absorption spectra were captured using HP 8453 UV-visible spectroscopy system, Germany. Moreover, the surface scanning of the Ni-rGO/TiO_2 nanocomposite has been detected using X-ray Photoelectron Spectroscopy (XPS, AXIS-NOVA, Kratos analytical Ltd, UK) with AlKα line of a 100 W X-ray tube as a radiation source and an energy of 20 eV. The scan rate was 0.5 eV/step, and a working pressure lower than 1×10^{-8} Nm^{-2}. The surface area and the average pore size of the Ni-rGO/TiO_2 nanocomposite are typically measured by the nitrogen adsorption BET method. They have been calculated by interpreting the adsorption isotherm of N_2 using Nova Station A 2200 surface area analyzer.

2.3 Photocatalytic activity for hydrogen production from water splitting

Photocatalytic water splitting reaction has been conducted in a 250 ml conical flask with a side opening and a stopper. The experiment starts by put in 50 mg of the catalyst in methanol/water mixture (75 ml water: 25 ml methanol, as a scavenger). Stirring is done to reduce the effect of

Preprints (www.preprints.org) | NOT PEER-REVIEWED | Posted: 10 February 2020 doi:10.20944/preprints202002.0129.v1

the hydrodynamic boundary layer around each nanocatalyst particle. Like so, it stimulates the gas disconnect after generation during the photocatalytic reaction. The H_2/ O_2 gases pass through the side opening of the flask and collect over the water in an inverted graduated cylinder. The rate of volume increase with time is recorded, and the volume of accumulated hydrogen is calculated. The experiments have been done under solar irradiation from 12:00~13:00 in June 2019 in Minia City, Egypt. (Latitude: 28° 06' 35.6" N Longitude: 30° 45' 1.1" E). The experiments have been done in successive days at the same time to reduce the effect of variation of solar intensity.

3. Results and discussion

3.1 The physical characterization of the Ni-rGO/TiO_2 nanocomposite

The surface morphology of the prepared Ni-rGO/TiO2 nanocomposite is shown in Fig. 1(a). It can be observed that the rGO layer appears with scattered irregular spots of Ni and TiO2 nanoparticles. This arbitrary distribution of the NPs through the rGO sheet can generate local active sites to facilitate the photocatalytic reactions. Figure 1(b) shows the HR TEM image of the prepared nanocomposite. It is evident that rGO appears as a layer with nanoparticles intercalated inside it. It seems that the dark spots are rich in Ni atoms while the gray is rich in TiO2 molecules. Figure 1(c) displays the EDX analysis of the samples. It can be noticed the appearance of C, Ti, and Ni with atomic % of 41.3, 8.97, and 18.3 %, respectively. However, this data is typically used to prove the presence of the element, not its actual distribution as the sampling area of the EDX is limited. Also, the figure misjudges the exact content of oxygen attached to both carbon and titanium atoms due to the nature of EDX very sensitive analysis to contamination.

Preprints (www.preprints.org) | NOT PEER-REVIEWED | Posted: 10 February 2020 doi:10.20944/preprints202002.0129.v1

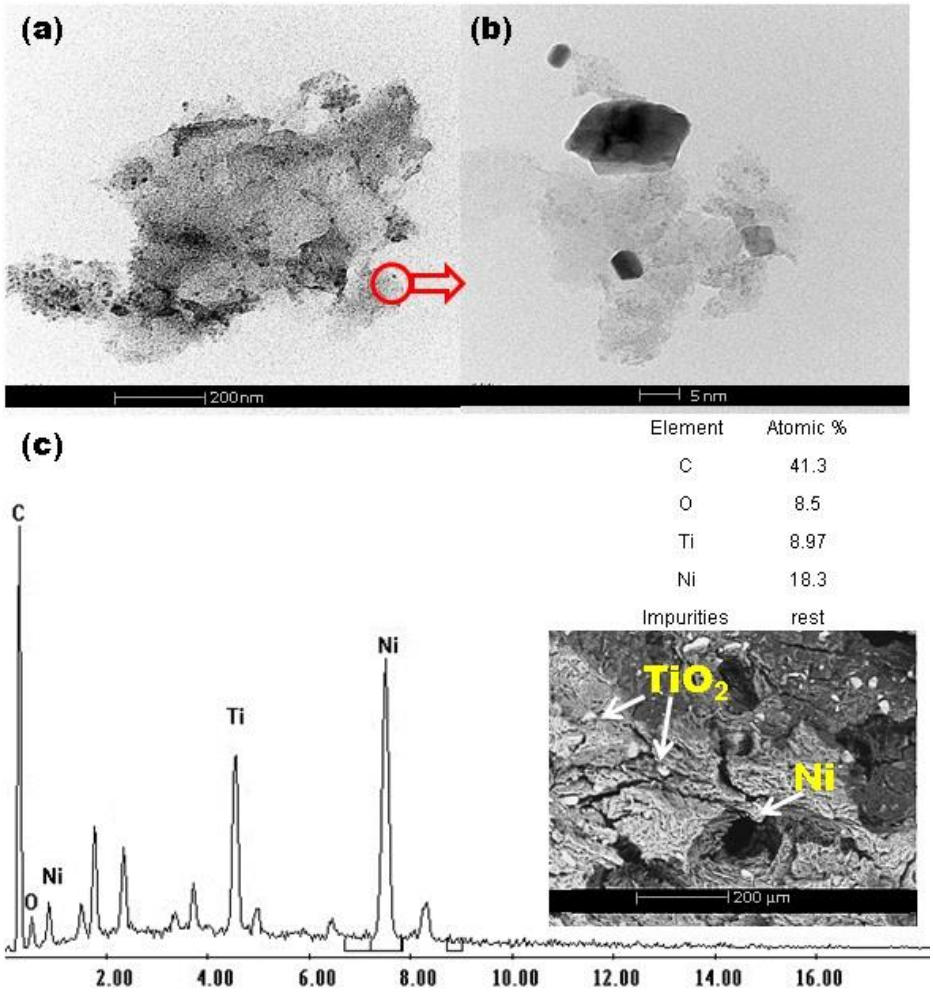

Fig. 1: (a) TEM image of Ni-rGO/TiO_2 nanocomposite rGO:TiO_2: Ni= 10: 1: 2, (b) HR TEM of the circled area of (a) sample indicating the presence of nanoparticles inside the rGO layer, (c) The EDS of Ni-rGO/TiO_2 nanocomposite (rGO: TiO_2: Ni = 10:1: 2), inset: SEM image of the same sample indicating white and dark spots.

The permeability of the prepared nanocomposite is typically calculated through the nitrogen adsorption/desorption cycle. The average pore size is important to indicate the tendency of the reactants and products to efficiently pass through the pores to the active sites. The BET surface area analysis is shown in Table 1. Remarkably, the Ni-rGO/TiO_2 nanocomposite sample exhibits a higher surface area than the commercial GO or the pristine rGO. This can be explained by the effect of the thermal treatment of the photocatalyst. Which doesn't merely increase the surface area, but also reduce the average pore size.

Preprints (www.preprints.org) | NOT PEER-REVIEWED | Posted: 10 February 2020 doi:10.20944/preprints202002.0129.v1

Table 1: BET surface area analysis of the prepared Ni-rGO/TiO_2 nanocomposite compared with other samples.

Material	Specific surface area m^2/g	Average diameter of the pores (nm)	Total specific pore volume cc/g	Ref.
TiO_2 nanoparticles	186.25	5	0.11	[25]
rGO	119.36	6.1	0.26	[27]
rGO-TiO_2	69.1	2.9	0.62	[27]
GO	25.38	5.5	0.1	[28]
Ni-rGO/TiO_2	224.4	9.9	0.11	This work

The XRD patterns of the prepared nanocomposite compared to rGO and GO is depicted in Figure 2(a). Regarding GO, the main diffraction peak at $2\theta = 10.1^o$ matching crystal planes of (0 0 2) appears in the sample. It reveals the effective oxidation of the graphite to GO as indicated by Xiong B., et al. [29]. For rGO sample, the dominant peak at $2\theta = 24.81^o$ revealed the formation of the honeycomb structure of the graphene layer. As for the Ni-rGO/TiO_2 nanocomposite, new peaks appeared to reveal the presence of Ni and TiO_2. The existence of TiO_2 diffraction peaks at 2θ values of 9.8^o, 27.8^o, and 48.2^o matches the crystal planes of (2 0 0), (3 1 0), and (0 2 0) of anatase, respectively (JCPDS card no 27-0124). However, the strength of the observed TiO_2 peaks are relatively lower than what expected from pure anatase. The reason for that is the effect of the calcination step, which breaks down the crystal structure within the sample and relatively weakens its sharp edges [26]. Furthermore, the peak appeared at 2θ values of 42.9^o could be attributed to the presence of either Ni or NiO according to the JCPDS cards no (04-0850 and 44-1159), respectively. A discrete reason emerged from that is the calcination step has a significant effect on the degree of the reduction of the Ni acetate precursor of the Ni nanoparticles. The decomposition of the acetate group can lead to the formation of NiO in the presence of oxygen and to Ni in the inert gas calcination process [26]. Actually, our calcination step has been conducted in vacuum at 850^oC. Then, we expect that the calcination step produced more Ni than

Preprints (www.preprints.org) | NOT PEER-REVIEWED | Posted: 10 February 2020 doi:10.20944/preprints202002.0129.v1

NiO nanoparticles. Incorporating the rGO with Ni and TiO_2 atoms induced the formation of small size crystals and decreased the degree of crystallinity.

Turning to the visible light absorbance of the prepared nanocomposite, the performance of the prepared nanocomposite compared to pure TiO_2 anatase is depicted in Fig. 2(b). The major absorption edge (λ_{abs}) for anatase can be obtained at 385 nm, which matches a bandgap of 3.2 eV [27]. By comparing the spectrum of both pure TiO_2 with that of Ni/rGO-TiO_2 nanocomposites, it is clear that a redshift to the visible region has been observed. The presence of transition metals broadened the absorption edge of the Ni-rGO/TiO_2 nanocomposite. This finding is one of the potential reasons for the better performance of the Ni-rGO/TiO_2 nanocomposite compared to both the rGO and the TiO_2. The redshift in the bandgap is observed due to the improved crystallinity of the Ni-rGO/TiO_2 nanocomposite. The optical bandgap of the film decreases with the increase in grain size. The barrier height of the grain boundary increases with the increase in grain size causing a decrease in the bandgap of the prepared sample.

The Tauc equation [28] can be used to calculate the direct bandgap of the Ni-rGO/TiO_2 nanocomposite. The inset of Fig. 2(b) shows the Tauc plot of $(\alpha h\upsilon)^2$ versus photon energy at direct allowed bandgap n=4. The linear part of the plot can be extended to determine the bandgap. The bandgap of Ni-rGO/TiO_2 nanocomposite is 2.7 eV. Typically, the new equilibrium state of Fermi level will promote the extension of e/h lifetime in the presence of transition metal oxide inside the p-type rGO and due to the synergy effect of forming a heterojunction with the n-type TiO_2.

Preprints (www.preprints.org) | NOT PEER-REVIEWED | Posted: 10 February 2020 doi:10.20944/preprints202002.0129.v1

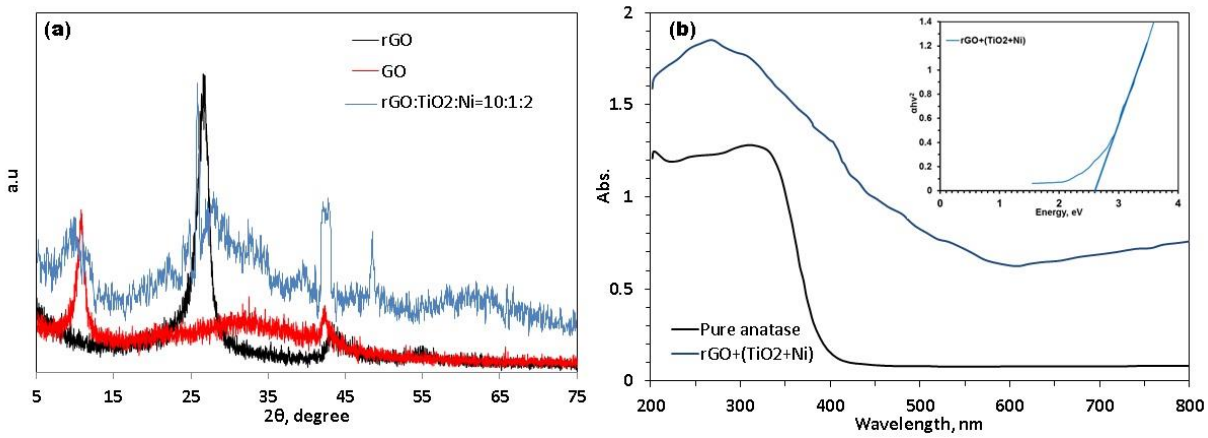

Fig. 2. (a) The XRD patterns of the prepared Ni-doped rGO incorporated TiO_2 nanoparticles, pure rGO, and pure GO. (b) UV-visible absorbance spectra for pure anatase and Ni-rGO/TiO_2 nanocomposite (rGO:TiO_2: Ni = 10:1:2). Inset: Tauc plot for calculation of direct band gap energies of Ni-rGO/TiO_2 nanocomposite.

To verify the presence of Ni and Ti incorporated in the rGO texture, the XPS analysis has been conducted. This analysis also identifies the chemical status of the dopant elements. Figure 3(a) presents the XPS survey spectrum of the Ni-rGO/TiO_2 nanocomposite. The spectrum showed the presence of Ti, O, Ni, C, Na and S elements. The sharp photoelectron peaks appeared at binding energies of 532 (O 1s) and 284 eV (C 1s), while weak photoelectron peaks appeared at 459 (Ti 2p), 857 eV (Ni 2p), and 169.8 (S 2p). The S and Na peaks are perhaps from external accidental sources such as dust and dirt or XPS instrument itself. Figure 3(b) exhibits the high-resolution XPS spectrum of the C 1s peak. It shows that the peak at 284.46 eV, this broad structure of the main C=C, and C-OH at 284.37 eV, and 285.46 eV. Figure 5(c) displays the split spin-orbit components of Ti2p spectrum. It indicates two non-symmetric peaks, the sharp one at 459.06 eV (corresponding to Ti $2p_{3/2}$) and a relatively small peak at 464.75 eV (corresponding to Ti $2p_{1/2}$), respectively. According to the Coster-Kronig effect, the post-ionization state of $Ti2p_{1/2}$ is short-lived compared to $Ti2p_{3/2}$ state. These outcomes are in line with the previous studies shown in [29, 30]. As confirmed in Fig. 3(d), the presence of the oxygen could be attributed to Ti attachment or rGO active sites. The presence of trace oxygen atoms in the rGO nanocomposite enhances carbon to carbon bonds and confirms the high quality of reduction. Figure 3(d) displays the O1s spectrum. The main peak observed at 532 eV corresponding to the metal oxide bond. Figure 3(e) demonstrates two significant binding energy peaks at 856.8 and 873.9 eV, respectively. These values signify the presence of $Ni2p_{3/2}$ and Ni $2p_{1/2}$ orbital states.

Preprints (www.preprints.org) | NOT PEER-REVIEWED | Posted: 10 February 2020 doi:10.20944/preprints202002.0129.v1

Accordingly, these peaks suggest the formation of $Ni(OH)_2$ in phase. Although Ni is bonded to the OH^-, The influence of the OH^- is caused by charge transfer from valence band bonding orbitals of OH^-, to unoccupied conduction band orbitals localized on Ni photo ions. Relaxation energy resulting from charge transfer is acquired by the emitted photoelectron.

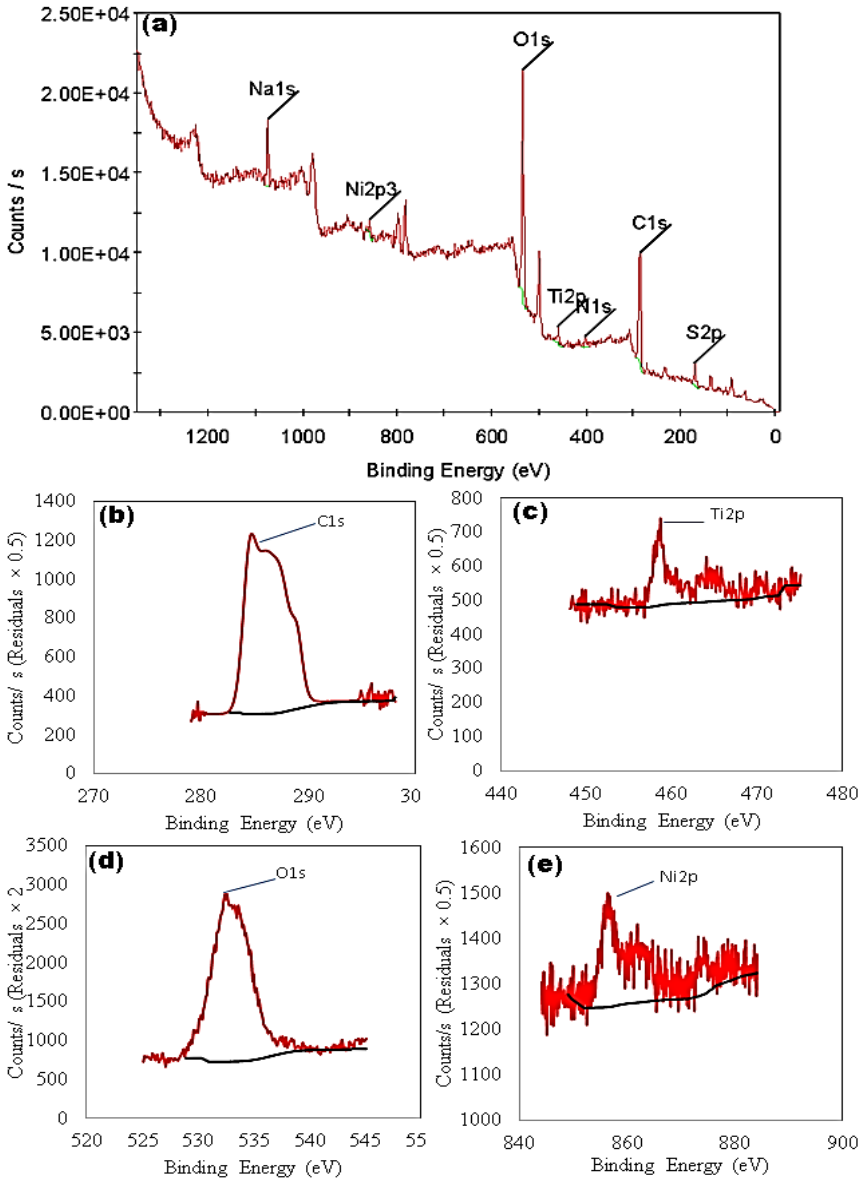

Fig. 3: (a) XPS panel of Ni-rGO/TiO_2 nanocomposite, (b) C1s peak, (c) Ti2p peak, (d) O1s peak, and (e) Ni 2p peak.

Preprints (www.preprints.org) | NOT PEER-REVIEWED | Posted: 10 February 2020 doi:10.20944/preprints202002.0129.v1

3.2 The photons-induced hydrogen generation

As the nanocomposite photocatalysts should work under visible solar radiation, the experiments have been conducted outdoor on sunny days. Typically, methanol is added to water as a scavenger component that does not interfere with the photocatalytic reaction. Its role in the photocatalytic water splitting is to quicken the hydrogen combination and evolution steps. Actually, methanol facilitates the electron injection to the conduction band according to the following mechanism [31].

$$CH_3OH + h^+ \rightarrow {}^*CH_2OH + H^+ \quad (4)$$

$$^*CH_2OH \rightarrow CH_2O + H^+ + e^- \quad (5)$$

On the rGO surface, methanol will not react with the holes. Alternatively, it will react with the OH radicals as follow:

$$^*OH + CH_3OH \rightarrow {}^*CH_2OH + H_2O \quad (6)$$

Figure 4(a) displays the specific volume of hydrogen generated as a function of time for different ratios of Ni loading (rGO:TiO_2: Ni = 10:1: 1~5). The volume of H_2 has been calculated from the volume change observed over the water level. It is evident from Fig. 5(a) that the ratio 10:1:4 (rGO: TiO_2: Ni) exhibited a comparatively better evolution rate of 18.2 ml H_2 min^{-1} $g^{-1}_{catalyst}$. Further addition of Ni nanoparticles showed a less rate of hydrogen production. In all the prepared samples, the volume of the collected hydrogen is a linearly time-dependent function. This reflects the stable activity of the prepared nanocomposite photocatalysts.

Preprints (www.preprints.org) | NOT PEER-REVIEWED | Posted: 10 February 2020 doi:10.20944/preprints202002.0129.v1

As verified by XPS, Ni should attach to the oxygen/ hydroxide functional groups over the rGO sheet. The NiO is a p-type semiconductor with a bandgap 3.6 eV, while TiO_2 is n-type with a bandgap 3.2 eV [32, 33]. A combination of p-n couples over the rGO sheet significantly improves the captivation of visible spectrum of the solar beams. Also, it extends the recombination time between the charge carriers (e/h). An arbitrary mechanism is shown in Fig. 5. Typically, rGO represents the main constituent of the prepared nanocatalyst. Due to the preparation method, the rGO surface should contain several oxygen-functional groups partially attached to the surface with a π- π bond. The valence band is adjusted to the O 2p orbitals, causing a broader bandgap for rGO. Whereas the conduction band of rGO contains some antibonding π-orbitals (viz., π*-orbitals)[4]. On the other side, the n-type TiO_2 provides more electrons that can easily go to the conduction band, as the energy level between the donor and the acceptor is low. They tend to form more levels above the Fermi level, thus skewing the electron distribution higher, therefore, the Fermi level moves upward. Contrarily, in the case of the p-type Ni-doped rGO, more energy levels closer to the valence band are added, they can accept an electron from the valence band, leaving a hole in the valence band. Thus, there are more energy levels below the Fermi level, which skews the Fermi level down closer to the conduction band according to the Fermi function equation:

$$f = \frac{1}{1+e^{(E-E_f)/k_B T}} \tag{7}$$

The quantum efficiency (QE) of photocatalytic water splitting to generate hydrogen can be expressed as: [34,35]

$$QE = \frac{Energy\ associated\ \ with\ H_2\ gas}{incident\ light\ intensity} = \frac{r_{H_2} \times \Delta G^o_{H_2O}}{I \times A} \tag{8}$$

Preprints (www.preprints.org) | NOT PEER-REVIEWED | Posted: 10 February 2020 doi:10.20944/preprints202002.0129.v1

where, r_{H_2} is the hydrogen production rate (mol s^{-1}), $\Delta G^{o}_{H_2O}$ is the standard Gibbs free energy for hydrogen production (J mol^{-1}), I is the incident light intensity (~ 262 W m^{-2} in Minia City, Egypt [36])), and A is the subjected area (cm^2). The Gibbs free energy needed to produce one mole of hydrogen from water (237.1 kJ mol^{-1}). The calculation of the efficiency of photocatalytic water splitting based on the value of r_{H_2}= 24.9 ml g_{cat}^{-1} min^{-1} reached 42.1%. Actually, the adopted nanocomposite photocatalyst load should be taken into account. However, any direct comparison between the photoactivity (μmol H_2 $g^{-1}_{catalyst}$ s^{-1}) of various materials can be strained due to different operating conditions (i.e., effective specific light source).

The Stability of the nanocatalyst is a vital factor for its validation. Accordingly, we verified the stability of the nanocatalyst by performing the solar water-splitting reaction for eight runs. After each run, the nanocomposite catalyst is separated, dried and reused for the subsequence run. The results are shown in Fig. 4(b) specified the reproducibility of the photocatalyst to accelerate the photocatalytic water splitting reactions without losing its activity. Ideally, the rate of H_2 evolution should be constant. However, the H_2 production rate, which is represented by the slopes of the line in Fig 5(b), increased as the runs proceed. This perhaps attributed to the sequence of reaction/separation/drying processes expose more active sites of the photocatalyst to be ready for the succeeding photocatalytic reaction. This finding indicates good stability for the photocatalysts. Accordingly, the rates of H_2 production emphasize the high efficiency as well as better durability of the introduced Ni-rGO/TiO_2 nanocomposite.

Preprints (www.preprints.org) | NOT PEER-REVIEWED | Posted: 10 February 2020 doi:10.20944/preprints202002.0129.v1

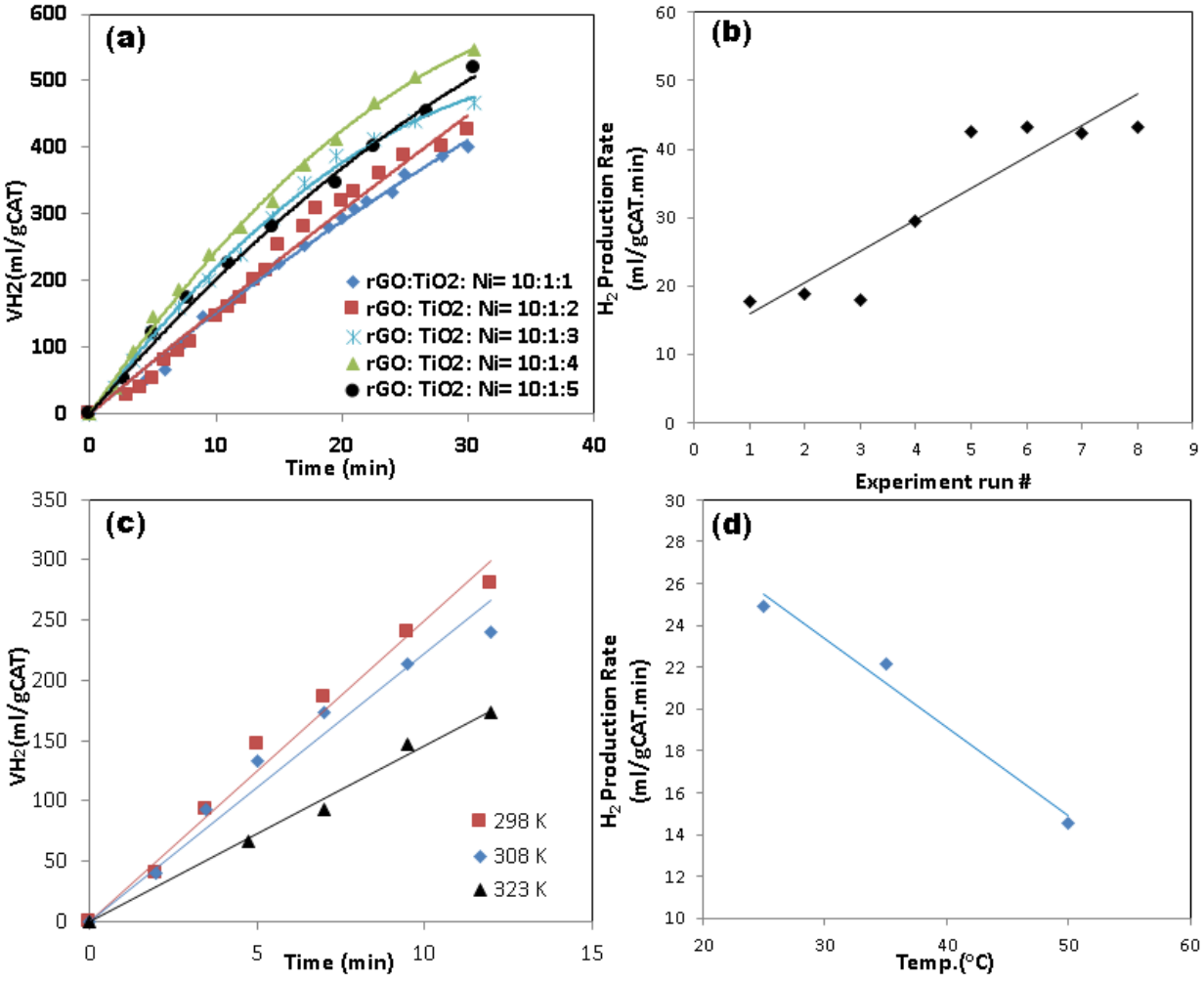

Fig. 4. The hydrogen specific evolution as a function of time for: (a) different Ni-doped rGO incorporated TiO_2 nanoparticles (rGO:TiO_2: Ni = 10:1: 1~5), (b) hydrogen evolution rate for 8 runs of the same Ni-rGO/TiO_2 nanocomposite (rGO:TiO_2: Ni = 10:1:4). (c) The hydrogen evolution as function of temperature for Ni-rGO/TiO_2 nanocomposite (rGO:TiO_2: Ni = 10:1:4). (d) the hydrogen production rate at different tempertaures.

3.3 The kinetic study

It is common knowledge that chemical reactions occur more rapidly at higher temperatures. Thermal energy relates directly to motion at the molecular level. As the temperature rises, molecules move faster and collide more vigorously, greatly increasing the likelihood of bond cleavages and rearrangements. Whether it is through the collision theory or transition state theory, chemical reactions are usually expected to be sensitive to the temperature change.

Preprints (www.preprints.org) | NOT PEER-REVIEWED | Posted: 10 February 2020 doi:10.20944/preprints202002.0129.v1

Arrhenius equation is typically used to calculate the reaction rate constants. The equation predicts that a small increase in reaction temperature will produce a marked increase in the magnitude of the reaction rate constant.

$$k = Ae^{-\frac{-E_A}{RT}} \quad (9)$$

where *K* is the chemical reaction rate constant, *A* is the pre-exponential factor or frequency factor; it represents the frequency at which atoms and molecules collide in a way that leads to reaction. Put differently, it means all the reactants molecules hold enough energy to form the products. E_a is the activation energy is the threshold energy that the reactant(s) must acquire before reaching the transition state. *R* is the gas constant, and *T* is the absolute temperature at which the reaction takes place. Figure 4(c) shows the rate of hydrogen generation at different reaction temperatures. It is noticeable that the rate of hydrogen generation decreases as the temperature rise. In addition, Fig. 4(d) shows the relation between the reaction rate and temperature. The slope of the curve is negative, indicating that the net reaction is barrierless. Accordingly, the activation energy has been calculated to be -17.6 kJ mol^{-1}. The calculated value is higher than that obtained by Hisatomi T, et al [37] who calculated the activation energy to split water using $Rh_{2-y}Cr_yO_3/(Ga_{1-x}Zn_x)(N_{1-x}O_x)$ catalyst. They found that the activation energy is 10 kJ mol^{-1} in the presence of ethanol scavenger and using Xenon lamp as a light source. Typically, the reactions involving charge transfer are denoted as barrierless reactions, in which the reaction only proceeds when the molecules are captured in a potential well. By increasing the temperature, it is expected that: i- the rate of photon conversion to heat increases, ii- the mobility of both charge carriers increases, iii- the recombination rate of e/h increases. Therefore, the probability of the water molecules to react over the catalyst surface will decrease.

It is worth mentioning that the photocatalytic reaction consists of several steps as shown in Table 2. The effect of temperature for the rate-controlling step will offset the adverse effect of the other relatively faster steps. In other words, the apparent activation energy for the water-splitting reaction reveals the activation energy of the slowest sub reaction stage. Those reaction stages involve photophysical steps and photoelectrochemical steps. Each is working simultaneously. The photophysical step involves the photon absorption, photoexcitation of the charge carriers, and charge motion. While the photoelectrochemical step includes the formation of chemical

Preprints (www.preprints.org) | NOT PEER-REVIEWED | Posted: 10 February 2020 doi:10.20944/preprints202002.0129.v1

bonds, a combination of charge carriers and ions, and water cleavage. The latter step has higher activation energies than the photophysical step. Contrarily, the rate of a photocatalytic reaction increases with increasing the intensity of photon excitation [26]. Some researchers suggest that the reaction order halfway decreases as the solar intensity increases. This reduction arises from the recombination of the charge carriers, which is second-order with respect to carrier concentrations.

Table 2: Steps of the photocatalytic reactions happening over the catalyst surface during the water cleavage.

Equation	Time scale	Comment	No.
$\mathbf{Ni-rGO/TiO_2} + h\nu \rightarrow Ni-rGO/TiO_2\ (e^- + h^+)$	fs	Upon excitation with solar radiation	(10)
$H_2O \rightarrow OH^- + H^+$	µs	Over the catalyst surface	(11)
$OH^- + h^+ \rightarrow O^- + H^+$	µs	Valance band reaction	(12)
$O^- + h^+ \rightarrow O$	s	Valance band reaction	(13)
$H^+ + e^- \rightarrow H$	µs	Conduction band reaction	(14)
$O_2 + e^- \rightarrow O_2^{\cdot -}$		Side reactions	(15)
$O_2^{\cdot -} + H^+ \rightarrow HO_2^{\cdot}$			(16)
$2HO_2^{\cdot} \rightarrow H_2O_2 + O_2$			(17)
$O_2^{\cdot -} + H_2O_2 \rightarrow OH^{\cdot} + OH^- + O_2$			(18)

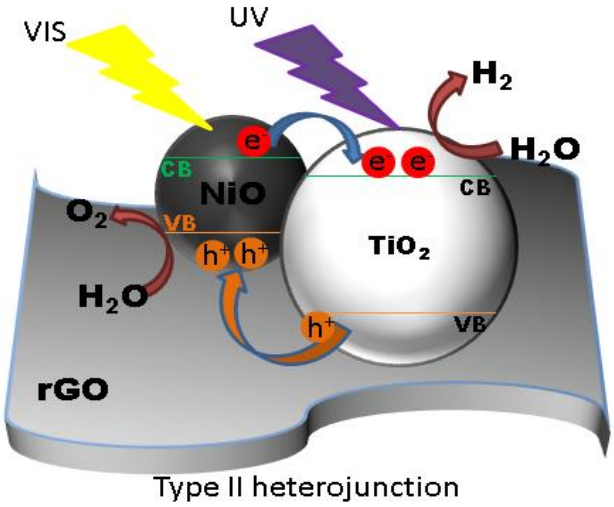

Type II heterojunction

Preprints (www.preprints.org) | NOT PEER-REVIEWED | Posted: 10 February 2020 doi:10.20944/preprints202002.0129.v1

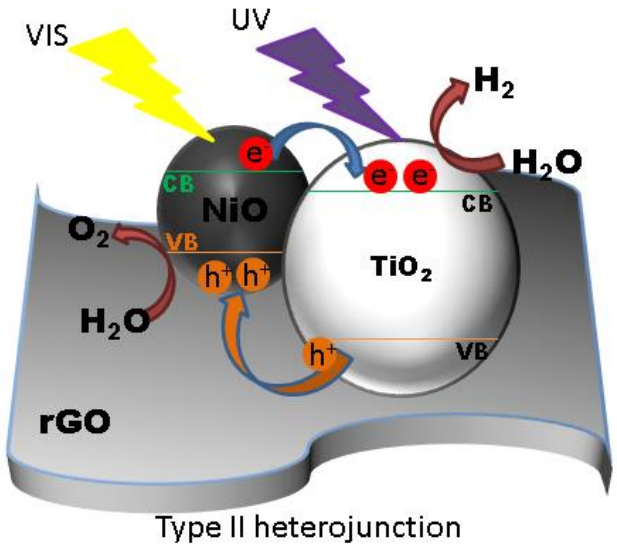

Fig. 5: An arbitrary mechanism for photocatalytic water cleavage over the rGO nanosheet

4. Conclusion

P-N heterojunction photocatalysis is an attractive and nonprecious alternative for photocatalytic water splitting. The present investigation has revealed the possibility of using Ni-rGO/TiO_2 nanocomposite for phpotocastalytic water splitting. TEM micrograph clearly indicates that the Ni and TiO_2 nanostructure succeeded to attach themselves to the rGO sheet in the lowest potential energy state. The EDS analysis gave a further indication of the existence of Ni and Ti elements within the composition of the nanocomposite photocatalyst. Further understanding of the surface morphology was accomplished by interpreting the XRD patterns. It revealed the presence of Ti, O, Ni, C, Na and S elements. However, the intensity of the Ti peaks was relatively weaker than that appeared in anatase XRD patterns due to the calcination effect. The XPS analysis revealed the presence of TiO_2 and Ni attached to the surface of the rGO sheet. Furthermore, UV–visible absorption spectroscopy demonstrates that the Ni-rGO/TiO_2 nanocomposite has an energy bandgap of 2.7 eV, which is a good indication for the reduction of the bandgap necessary for water cleavage. Experimentally, the optimum ratio of rGO:TiO_2: Ni was 10:1: 4 which showed better photocatalytic activity toward water splitting under the visible light irradiation. The reproducibility of the results using the same nanocatalyst showed better stability during 8 cycles. The kinetic study revealed that the reaction is a barrierless with negative activation energy.

References

[1] Miwa T, Kaneco S, Katsumata H, Suzuki T, Ohta K, Verma SC, et al. Photocatalytic hydrogen production from aqueous methanol solution with $CuO/Al_2O_3/TiO_2$ nanocomposite. Int J Hydrogen Energ. 35 (2010) 6554-60.

[2] Dougherty W, Kartha S, Rajan C, Lazarus M, Bailie A, Runkle B, et al. Greenhouse gas reduction benefits and costs of a large-scale transition to hydrogen in the USA. Energy policy. 37(2009)56-67.

[3] Alenzi N, Liao W-S, Cremer PS, Sanchez-Torres V, Wood TK, Ehlig-Economides C, et al. Photoelectrochemical hydrogen production from water/methanol decomposition using Ag/TiO_2 nanocomposite thin films. Int J Hydrogen Energ. 35 (2010)11768-75.

[4] Yeh T-F, Cihlář J, Chang C-Y, Cheng C, Teng H. Roles of graphene oxide in photocatalytic water splitting. Mater Today. 16(2013) 78-84.

[5] Luca Bertoluzzi, Pilar Lopez-Varo, Juan Antonio Jiménez Tejada, Juan Bisquert, Charge transfer processes at the semiconductor/electrolyte interface for solar fuel production: insight from impedance spectroscopy, J. Mater. Chem. A, 4 (2016) 2873-2879.

[6] Wu¨rfel P, Wu¨rfel U (2009), "Physics of solar cells, from basic principles to advanced concepts", Wiley 1st ed., pp 106-120.

[7] M. De Laurentis, A. Irace, Optical measurement techniques of recombination lifetime based on the free carriers absorption effect, J Solid State Phys. 2014 (2014) Article ID 291469, http://dx.doi.org/10.1155/2014/291469.

[8] Mohamed S. Mahmoud, Enas Ahmed, A.A. Farghali, A.H. Zaki, Nasser A.M. Barakat, Synthesis of Fe/Co-doped titanate nanotube as redox catalyst for photon-induced water splitting, Mater Chem Phys. 217(2018)125–132.

[9] Mohamed S. Mahmoud, Enas Ahmed, A.A. Farghali, A.H. Zaki, Emad A.M. Abdelghani,Nasser A.M. Barakat, Influence of Mn, Cu, and Cd–doping for titanium oxide nanotubes on the photocatalytic activity toward water splitting under visible light irradiation, Colloids and Surfaces A: Physicochemical and Engineering Aspects, 554(5) (2018) 100–109.

[10] Fujishima A, Honda K. Electrochemical photolysis of water at a semiconductor electrode. Nature. 238(1972) 37-38.

[11] Cheng P, Yang Z, Wang H, Cheng W, Chen M, Shangguan W, et al. TiO_2–graphene nanocomposites for photocatalytic hydrogen production from splitting water. Int J Hydrogen Energ. 37(2012) 2224-30.

[12] Yoong L, Chong FK, Dutta BK. Development of copper-doped TiO_2 photocatalyst for hydrogen production under visible light. Energy. 34(2009) 1652-61.

[13] Li L, Yan J, Wang T, Zhao Z-J, Zhang J, Gong J, et al. Sub-10 nm rutile titanium dioxide nanoparticles for efficient visible-light-driven photocatalytic hydrogen production. Nature communications. 6(2015) 5881.

[14] Asahi R, Morikawa T, Ohwaki T, Aoki K, Taga Y. Visible-light photocatalysis in nitrogen-doped titanium oxides. Science. 293(2001)269-71.

[15] Sakthivel S, Kisch H. Daylight photocatalysis by carbon-modified titanium dioxide. Angewandte Chemie International Edition. 42(2003) 4908-11.

[16] Chen X, Burda C. The electronic origin of the visible-light absorption properties of C-, N-and S-doped TiO_2 nanomaterials. J Am Chem Soc. 130(2008)5018-9.

[17] Rongchen Shen, Jun Xie, Quanjun Xiang, Xiaobo Chen, Jizhou Jiang, Xin Li, Ni-based photocatalytic H_2-production cocatalysts, Chinese Journal of Catalysis, 40 (2019) 240-288

[18] Xin Li,Rongchen Shen, Song Ma, Xiaobo Chen, Jun Xie, Graphene-based heterojunction photocatalysts Applied Surface Science, 430 (2018) 53-107.

[19] Wang D, Choi D, Li J, Yang Z, Nie Z, Kou R, et al. Self-assembled TiO_2–graphene hybrid nanostructures for enhanced Li-ion insertion. ACS nano. 3(2009)907-14.

[20] Zhang X-Y, Li H-P, Cui X-L, Lin Y. Graphene/TiO_2 nanocomposites: synthesis, characterization and application in hydrogen evolution from water photocatalytic splitting. J Mater Chem. 20(2010) 2801-6.

[21] Tomoaki Takayama, Ko Sato, Takehiro Fujimura, Yuki Kojima, Akihide Iwasea and Akihiko Kudo, Photocatalytic CO_2 reduction using water as an electron donor by a powdered Z-scheme system consisting of metal sulfide and an rGO–TiO_2 composite, Faraday Discussions, DOI: 10.1039/c6fd00215c.

[22] Rajni Garg, Naba K. Dutta and Namita Roy Choudhury, Work function engineering of graphene, Nanomaterials, 4(2014) 267-300.

[23] X. Y. Zhang, H. P. Li, X. L. Cui, Y. Lin, Graphene/TiO_2 nanocomposites: synthesis, characterization and application in hydrogen evolution from water photocatalytic splitting, J. Mater. Chem. 20 (2010) 2801-806.

[24] X. Zhang, Y. Sun, X. Cui, Z. Jiang, A green and facile synthesis of TiO_2/graphene nanocomposites and their photocatalytic activity for hydrogen evolution, Int. J. Hydrogen Energy. 37(1) (2012) 811-815.

[25] Xiuzhen Wei, Guangfeng Zhu, Jinfeng Fang, and Jinyuan Chen, Synthesis, characterization, and photocatalysis of well dispersible phase-pure anatase TiO_2 nanoparticles, Int J Photoenergy, 2013, Article ID 726872, DOI: http://dx.doi.org/10.1155/2013/726872.

[26] Juan C. De Jesus, Ismael Gonz´alez, Angel Quevedo, Tito Puerta, Thermal decomposition of nickel acetate tetrahydrate: an integrated study by TGA, QMS and XPS techniques, J Mol Catal A-Chem. 228 (2005) 283–291.

[27] Hoffmann MR, Martin ST, Choi W, Bahnemann DW. Environmental applications of semiconductor photocatalysis. Chem rev. 95(1995) 69-96.

[28] M. M. Momeni, Y. Ghayeb, Visible light-driven photoelectrochemical water splitting on ZnO–TiO_2 heterogeneous nanotube photoanodes, J. Appl. Electrochem., 45 (2015) 557-566.

[29] Y. Ma, Y. Li, D. Li, Y. Liu, and J. Zhang, Uniformly distributed TiO_2 nanorods on reduced graphene oxide composites as anode material for high rate lithium ion batteries, J Alloys Compd. 771(2019) 885-891.

[30] L. Song, L. Li, X. Gao, J. Zhao, T. Lu, and Z. Liu, A facile synthesis of a uniform constitution of three-dimensionally ordered macroporous TiO_2–carbon nanocomposites with hierarchical pores for lithium ion batteries, J Mater Chem *A*, 3(2015) 6862-72.

[31] F. Guzman, S.S. Chuang, C. Yang, Role of methanol sacrificing reagent in the photocatalytic evolution of hydrogen, Industrial & Engineering Chemistry Research, 52 (2012) 61-65.

[32] Wu N-L, Lee M-S. Enhanced TiO_2 photocatalysis by Cu in hydrogen production from aqueous methanol solution. Int. J Hydrogen Energ. 29 (2004)1601-5.

[33] Sreethawong T, Suzuki Y, Yoshikawa S. Photocatalytic evolution of hydrogen over mesoporous TiO_2 supported NiO photocatalyst prepared by single-step sol–gel process with surfactant template. International journal of hydrogen energy. 30 (2005)1053-62.

 doi:10.20944/preprints202002.0129.v1

[34] Maeda, K. Photo-catalytic water splitting using semiconductor particles: History and recent developments. J. Photochem. Photobiol. C Photochem. Rev. 12 (2011) 237–268.

[35] Qureshi, M.; Takanabe, K. Insights on measuring and reporting heterogeneous photocatalysis: Efficiency definitions and setup examples. Chem. Mater. 29 (2016) 158–167.

[36] M. Bady, Towards sustainable power generation using solar chimney, OALib Journal, 2 (2015) 1.

[37] Hisatomi T, Maeda K, Takanabe K, Kubota J, Domen K, Aspects of the water splitting mechanism on $(Ga_{1-x}Zn_x)(N_{1-x}O_x)$ photocatalyst modified with $Rh_{2-y}Cr_yO_3$ cocatalyst, J Phys Chem C. 113(51) (2009) 21458-21466.